First-principles study for ordering and phase separation in the Fe-Pd system

2002 J. Phys.: Condens. Matter 14 1903

(http://iopscience.iop.org/0953-8984/14/8/318)

INSTITUTE OF PHYSICS PUBLISHING JOURNAL OF PHYSICS: CONDENSED MATTER

J. Phys.: Condens. Matter **14** (2002) 1903–1913 PII: S0953-8984(02)29171-7

First-principles study for ordering and phase separation in the Fe–Pd system

Ying Chen[1], **Takaharu Atago**[1] **and Tetsuo Mohri**[2]

[1] Materials and Chemical Substances Information Division, Department of Advanced Databases, Japan Science and Technology Corporation, 5-3 Yonban-cho, Chiyoda-ku, Tokyo, 102, Japan
[2] Division of Materials Science and Engineering, Graduate School of Engineering, Hokkaido University, Kita-13 Nishi-8, Kita-ku Sapporo, 060-8628, Japan

E-mail: ying@tokyo.jst.go.jp

Received 26 September 2001, in final form 11 January 2002
Published 15 February 2002
Online at stacks.iop.org/JPhysCM/14/1903

Abstract

The main features of the phase diagram of the Fe–Pd system are characterized by phase separation in the Fe-rich region and appearance of two ordered phases in the Pd-rich region. The total-energy FLAPW electronic structure calculations are attempted on a set of selected ordered compounds as well as Fe and Pd to clarify the origin of these features. It is revealed that (i) magnetism plays a dominant role in the phase stability of the system and (ii) the system has an intrinsically large driving force for ordering, while the elastic energy originating from size mismatch causes the phase separation in the Fe-rich portion.

1. Introduction

Recently, the Fe–Pd system has been attracting broad attention due to excellent heat resistant properties at elevated temperatures. Based on electron microscopy observation [1], it has been revealed that the coherent precipitates of $L1_0$ ordered phase distributed in the ferrite matrix are responsible for improving the creep resistance. One of the present authors attempted phenomenological calculation [2] of $L1_0$-disorder phase equilibria based on phenomenological Lennard-Jones-type pair potentials determined by experimental data of heats of formation, cohesive energies and lattice constants. Although the resultant phase diagram was quite reasonable and reproduced the transition temperature quite satisfactorily, such a phenomenological approach by no means clarifies the essential origin of the phase stability of the system. Following this preliminary calculation, the present study is undertaken to clarify the physical origin of the phase stability of the Fe–Pd system.

An experimental phase diagram of the Fe–Pd system [3] is characterized by three features. The first one is the broad phase separation in the Fe-rich region. Another is the appearances of two ordered phases with $L1_0$ and $L1_2$ structures near 1:1 and 1:3 stoichiometric compositions, respectively, and the last one is that the congruent composition of $L1_0$ ordered phase relatively shifts from 1:1 stoichiometry towards the Pd-rich portion.

The major purpose of the present electronic structure calculation is to reveal physical origins of these features. Although the final aim of the present study is to derive a phase diagram, this claims statistical mechanics calculation at finite temperatures and will be discussed in a separate paper [4]. Hence, this report is regarded as a precursor to the series of investigations for the phase equilibria in the Fe–Pd system. Its organization is as follows. In the next section, we briefly describe the procedure of theoretical calculations. The entire procedure of theoretical analyses is quite similar to that performed for noble alloy systems by Terakura *et al* [5]. The major results are presented and discussed in the third section.

2. Theoretical procedure

In view of the various magnetic transitions in the Fe-rich portion of an experimental phase diagram, it is desirable to derive magnetic interaction energies in addition to conventional atomic interaction energies. This is, however, anticipated to demand quite laborious calculations. Instead of explicitly introducing magnetic interactions, in this study we performed two types of total energy calculation, *spin-polarized* and *non-polarized* calculations on ferromagnetic (fm) and nonmagnetic (nm) structures, respectively.

First, we employed the full-potential linearized augmented-plane-wave (FLAPW) [6] method within the generalized gradient approximation (GGA) [7] to obtain the total energies $E_{\mathrm{Fe}_{4-n}\mathrm{Pd}_n}(r)$ for $\mathrm{Fe}_{4-n}\mathrm{Pd}_n$, where n is an integer value from zero to four, as a function of lattice constant r. The particular atomic arrangements we studied are fcc for $n = 0$ and 4, $\mathrm{L1}_2$ for $n = 1$ and 3 and $\mathrm{L1}_0$ for $n = 2$. It should be noted that both FePd and FePd_3 are stable phases whereas $\mathrm{Fe}_3\mathrm{Pd}$ is a hypothetical phase, which cannot be found in the equilibrium phase diagram. In view of the fact that the most stable ground state of Fe is the bcc-Fe with *ferro*magnetic state, we also performed the additional calculation to obtain $E^{\mathrm{bcc}}_{\mathrm{Fe}_4}(r)$. For all the calculations, the cutoff energies for the wavefunction and charge density expansion are 20.0 and 80.0 Ryd, respectively. The tetrahedron method is adopted for the k-space integration. The numbers of irreducible k points were 85 for fcc and 84 for $\mathrm{L1}_0$ and $\mathrm{L1}_2$ lattices. The convergence of total energy was carefully checked (<0.001 mRyd/formula unit), and it was assured that the convergence in the relative energy between different structures is an order of magnitude better than the convergence in the absolute total energy. It is noted that, since our main interest is fcc-based phases, Fe is an fcc structure throughout this study unless 'bcc' is specified.

With total energies $E_{\mathrm{Fe}_{4-n}\mathrm{Pd}_n}$, the heats of formation ΔE_n are obtained as

$$\Delta E_n(r) = E_{\mathrm{Fe}_{4-n}\mathrm{Pd}_n}(r) - \frac{4-n}{4}E^{\mathrm{bcc}}_{\mathrm{Fe}_4}(r_{\mathrm{bcc}}) - \frac{n}{4}E_{\mathrm{Pd}_4}(r_4), \tag{1}$$

where r_4 and r_{bcc} are the equilibrium lattice constants at which the total energies of E_{Pd_4} for Pd_4 and $E^{\mathrm{bcc}}_{\mathrm{Fe}_4}$ for bcc-Fe_4 take minimum values, respectively. Note that $E^{\mathrm{bcc}}_{\mathrm{Fe}_4}$ is the energy for four atoms. The operation given in equation (1) introduces the *segregation limit* as an energy reference state. The resultant ΔE_n is fitted in the Lennard-Jones-type potential expressed as

$$\Delta E_n(r) = \frac{a_n}{r^7} - \frac{b_n}{r^{3.5}} + c_n. \tag{2}$$

Then, the cluster expansion method (hereafter CEM) [8] is employed to extract effective cluster interaction energies, $v_m(r)$, up to a nearest-neighbour tetrahedron cluster. The key ingredient of the CEM is that a configuration-dependent energy $\Delta E_n(r)$ can be expanded in terms of a set of correlation functions $\{\xi^n_m\}$,

Table 1. Values of correlation functions.

	$m = 0$ Null	$m = 1$ Point	$m = 2$ Pair	$m = 3$ Triangle	$m = 4$ Tetrahedron
Fe	1	1	1	1	1
Fe_3Pd	1	1/2	0	−1/2	−1
FePd	1	0	−1/3	0	1
$FePd_3$	1	−1/2	0	1/2	−1
Pd	1	−1	1	−1	1

$$\Delta E_n(r) = \sum_{m=0}^{E_{\max}} v_m(r)\xi_m^n, \tag{3}$$

where m specifies a cluster and ξ_m^n is the correlation function defined as

$$\xi_m^n = \langle \sigma_{p_1}\sigma_{p_2}\cdots\sigma_{p_k}\cdots\sigma_{p_m}\rangle, \tag{4}$$

where σ_{p_k} is the spin operator, which takes either +1 or −1 depending upon the A or B atom located at the lattice point specified by p_k involved in the m-point cluster of the phase n, and $\langle\rangle$ suggests the ensemble average. Note that $m = 0$ corresponds to the *null* cluster. Although mathematical details are not provided in this report, it is proved [9] that a set of correlation functions spans the orthonormal bases in the thermodynamic configuration space, assuring the validity of the present expansion.

In the alloy thermodynamics, cluster probabilities are often employed to describe the atomic configuration. For instance, x_i and y_{ij} are most often encountered to represent point and pair cluster probabilities, respectively, of finding an atomic configuration specified by subscript(s). One can readily prove that these cluster probabilities are interrelated with a set of correlation functions through linear transformation [10, 11]. Instead of detailed mathematical discussions, we simply provide the following relationships, and interested readers should consult the original articles:

$$x_i = \tfrac{1}{2}\{1 + i\xi_1\} \tag{5}$$

and

$$y_{ij} = \frac{1}{2^2}\{1 + (i + j)\xi_1 + ij\xi_2\} \tag{6}$$

where i and j take either +1 or −1 for A and B atoms, respectively.

The values of correlation functions for the phases of interest in this study are provided in table 1. One sees that $\{\xi_m^n\}$ constitutes 5×5 matrix and it is readily confirmed that this is a regular matrix. The non-singularity of the matrix, $\{\xi_m^n\}$, is further guaranteed by the fact that the atomic arrangement of any phase n considered above cannot be geometrically synthesized by the combination of those of other phases involved in the table. Then, the matrix inversion of equation (3) yields the effective interaction energies,

$$v_m(r) = \sum_{n=0}^{4} \{\xi_m^n\}^{-1}\Delta E_n(r). \tag{7}$$

The upper limit of the summation, $E_{\max}$, in equation (3) specifies the largest cluster participating in the expansion. Since $\{\xi_m^n\}$ is the 5×5 matrix and the biggest cluster considered is the tetrahedron cluster as tabulated in table 1, $E_{\max}$ should be mathematically four, representing a nearest-neighbour tetrahedron cluster. Except for such a mathematical condition, the criterion of the choice of $E_{\max}$ is not well established, but in view of the fact that the contribution of the

Table 2. Equilibrium properties (equilibrium lattice parameter a_0, bulk modulus B_0 and pressure derivative of the bulk modulus B') and magnetic moments of five ordered phases by present calculation, and comparison with experimental data. It should be noted that Fe_3Pd is a hypothetical compound.

		a_0 (Å)	B_0 (GPa)	B'	M (μ_B/atom)
Fe	calc.—fm	3.485	198.9	6.6	1.05
	calc.—nm	3.449	298.7	7.1	
	exp.	3.648 [13], 3.666 [13]	168.3 [14]		
Fe_3Pd	calc.—fm	3.740	155.9	3.9	2.16 (Fe: 2.76, Pd: 0.36)
	calc.—nm	3.608	246.1	4.0	
FePd	calc.—fm	$a = 3.809$, $c = 3.771$	184.4	2.9	1.65 (Fe: 2.94, Pd: 0.35)
	calc.—nm	$a = 3.733$, $c = 3.643$	215.6	4.6	
	exp.	$a = 3.852$, $c = 3.723$ [13]	170 [15]		1.49 [15]
		$a = 3.855$, $c = 3.714$ [13]			
	other calc.	$a = 3.732$, $c = 3.672$ [18]			1.66 (Fe: 2.98, Pd: 0.34) [18]
$FePd_3$	calc.—fm	3.895	177.1	5.7	1.08 (Fe: 3.32, Pd: 0.34)
	calc.—nm	3.847	194.4	5.2	
	exp.	3.848 [13], 3.855 [13]			1.10 (Fe: 2.70, Pd: 0.57) [16]
					0.97(Fe: 2.86, Pd: 0.34) [17]
Pd	calc.—fm	3.931	182.2	5.4	0.18
	calc.—nm	3.931	182.0	5.4	
	exp.	3.887 [13], 3.890 [13]	180.8 [14]		

energies from truncated clusters are automatically renormalized in the extracted energies of smaller clusters, the convergence of the extracted effective cluster interaction energies should be carefully examined. This is discussed in the following section.

3. Results and discussion

By fitting the calculated total energies versus volume for various phases to Murnaghan's equation of state [12], we derived equilibrium properties such as lattice parameter a_0, bulk modulus B_0 and the pressure derivative of the bulk modulus B' from the equation of state. The results are summarized in table 2, together with magnetic moments and available experimental data [13–17]. Although the experimental data scatter somewhat, the agreements between our theoretical values and the experimental ones are fairly good. These are particularly pronounced for fm (*spin-polarized* calculation).

Shown in figures 1(a) and (b) are total energies, $\Delta E_n(r)$, of five phases as a function of lattice constant, r, obtained by spin-polarized and non-polarized FLAPW calculations, respectively. Drawn by a broken curve in figure 1(a) is $\Delta E^{\mathrm{bcc}}_{\mathrm{Fe}_4}(r)$, which defines the energy reference state of Fe_4. We note that the calculated lattice constant of bcc-Fe is 5.36 (au), which is quite small as compared with those of the other fcc-based phases. In order to facilitate the comparison of heats of formation of all the phases, we converted this value to an fcc-equivalent keeping the same atomic volume. One can clearly see that the spin-polarized calculation (figure 1(a)) predicts the correct tendency of the experimental phase diagram i.e. both the appearance of FePd and $FePd_3$ and the disappearance of Fe_3Pd. It is noted that the total energies $E_{\mathrm{Fe}_{4-n}\mathrm{Pd}_n}(r)$ for $Fe_{4-n}Pd_n$ ($n = 0$–3) with nm state are far higher than those with fm state. Hence, if we employ the same segregation limit in figure 1(a) keeping the same energy scale, a comparison for non-polarized calculations is obscured. Then, again in order to facilitate comparison for non-polarized calculation, we adopt the concentration

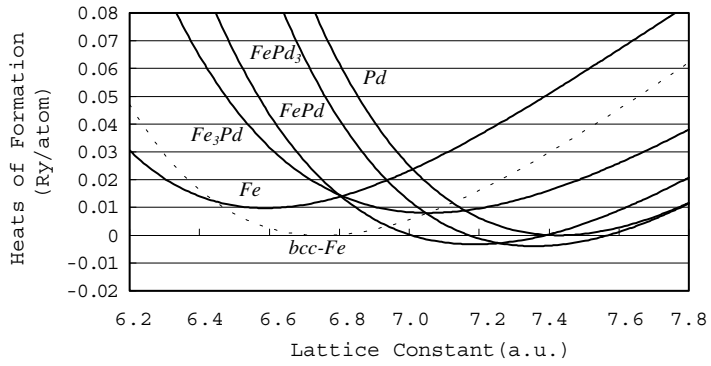

(a)

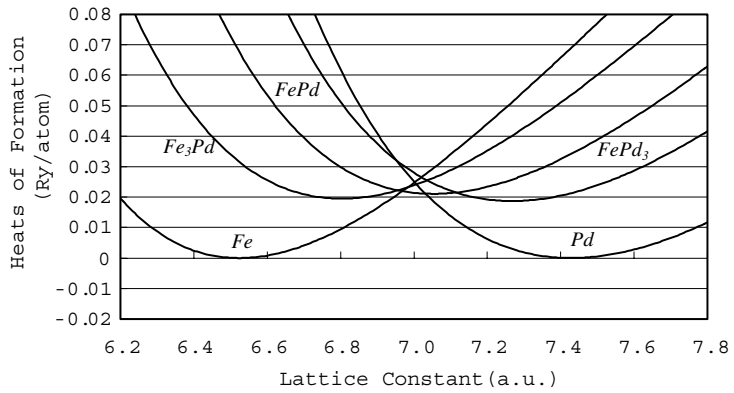

(b)

Figure 1. Heats of formation of Fe, Fe_3Pd, FePd, $FePd_3$ and Pd obtained by (*a*) spin-polarized and (*b*) non-polarized calculations as a function of lattice constant (atomic unit). The segregation limits are defined as the concentration average of total energies of bcc-Fe (fm) and Pd in (*a*), while those of fcc-Fe (nm) and Pd for (*b*). In (*a*) heats of formation of bcc-Fe (fm) are plotted by a broken curve after converting the lattice constant.

Table 3. Fitting parameters of heats of formation into Lennard-Jones-type potential via equation (2).

	$a_n(\times 10^5)$	$b_n(\times 10^2)$	c_n
Fe	1.9914	5.4245	0.3792
Fe_3Pd	2.9778	6.3843	0.3502
FePd	3.8528	7.7429	0.3843
$FePd_3$	5.2731	9.7599	0.4476
Pd	5.8723	10.514	0.4706

average of E_{Fe_4} with nm state and E_{Pd_n} as the segregation limit. In view of the fact that the total energy of fcc-Fe with nm state is far larger than those of fcc- and bcc-Fe with fm state, figure 1(*b*) suggests that the non-polarized calculation destabilizes all the ordered phases. These results clearly indicate the importance of magnetism for the phase stability in the Fe–Pd system. Hence, hereafter, our main focus is placed only on the results of spin-polarized calculation. The coefficient terms, a_n, b_n and c_n in equation (2) for each phase n are tabulated in table 3.

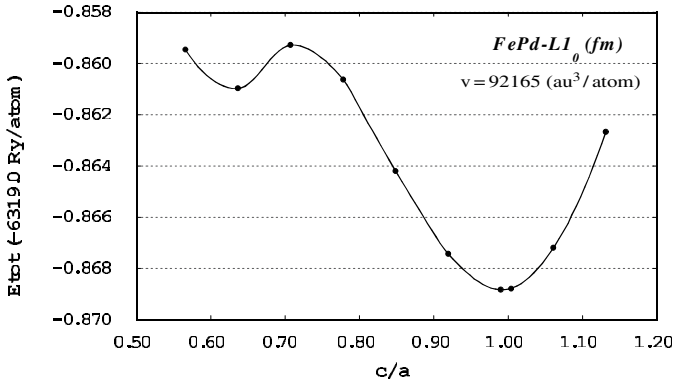

Figure 2. Total energy of $L1_0$ ordered phase as a function of tetragonality c/a.

As was pointed out at the beginning of the previous section, it is most desirable to separate out the magnetic interaction energies from the total heats of formation obtained above. The interplay between magnetic interaction and chemical interaction determines the relative position of the locus of Curie temperature and the phase boundary, which provides a clue to analyse the effects of magnetism on the order–disorder transition behaviour. Also, detailed calculations of magnetic interaction energies should be useful and desirable to understand the origin of the strong magnetocrystalline anisotropy of FePd [18], which has been attracting broad attention to develop magneto-optical devices. Such a calculation of magnetic interactions is initiated and will be reported elsewhere.

It is well known that tetragonality is often associated with the $L1_0$ ordered phase. Then the additional calculation is also attempted to obtain total energies of $L1_0$ ordered phase as a function of the tetragonality $\theta = c/a$, where a and c are the lattice constants of a tetragonal phase in the x (and y) and z directions, respectively. Note that in this coordinate system, (001) planes are alternatively occupied by either Fe or Pd atoms. The results are demonstrated in figure 2. One sees that the minimum appears at $\theta \approx 0.99$, which is in good agreement with the experimental value of 0.96–0.97 [13]. In view of the closeness to unity of the calculated θ, the following calculations and analyses are performed by neglecting the tetragonality.

Based on equation (7), CEM is operated on the total energies, and a set of effective cluster interaction energies, $\{v_m(r)\}$, is extracted. The results are shown in figure 3. One can see that three- and four-body interaction energies are quite small as compared with the pair interaction energy, which also confirms the convergence of the expansion. The major contribution of the pair interaction energy is a characteristic of a metallic alloy system of which cohesion is generally dominated by central forces.

The alternative first-principles approach to alloy thermodynamics including the calculation of a phase diagram is to start with the total-energy calculation for a complete random alloy by the coherent potential approximation (CPA) [19] followed by the generalized perturbation method (GPM) [20] to extract pair-wise interaction energies. Recent detailed investigation [21] on Coulomb energies in alloys points out the importance of the interatomic Coulomb energy and suggests that the long-range nature of the Coulomb interaction is well incorporated in the charge-consistent CPA [22]. In contrast, the present approach within the CEM is limited to the nearest-neighbour cluster interactions, and all the long-range pair interactions as well as many-body interactions beyond a nearest-neighbour tetrahedron cluster are renormalized in the extracted effective interactions. Hence, the details of atomic interactions may be obscured in the present CEM. Yet, two major reasons to employ the present scheme are addressed.

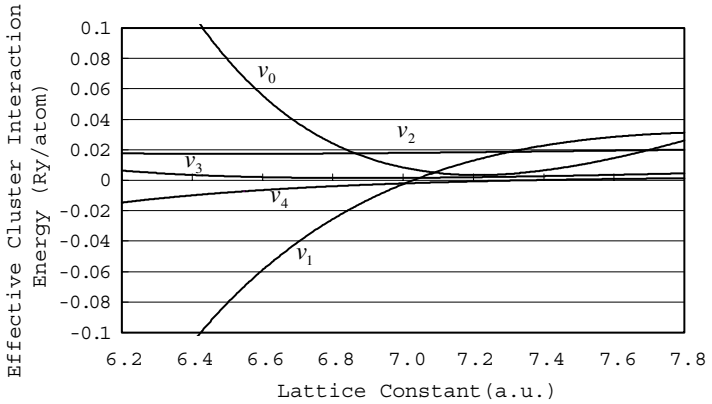

Figure 3. Effective cluster interaction energies up to the nearest-neighbour tetrahedron cluster. v_i represents an i-point cluster and $i = 0$ corresponds to a null cluster.

The first one is rather technical. The eventual purpose of the present investigation is to calculate a phase diagram, and a set of effective cluster interaction energies obtained here are incorporated into cluster variation method (hereafter CVM) [23]. Unfortunately, however, even the highest level of approximation of the CVM is only capable of incorporating interactions up to the fourth-nearest-neighbour pair. The common practice of the CVM is to employ the tetrahedron approximation in which cluster interactions and correlations up to the nearest-neighbour tetrahedron cluster can be considered. Hence, in view of such a limitation imposed by CVM, the present expansion is truncated at the nearest-neighbour tetrahedron cluster. The second reason is that, in the earlier investigation of the ground-state analysis [24], it was demonstrated that both $L1_0$ and $L1_2$ ordered phases, which are our main interests, can be stabilized within the nearest-neighbour pair interaction energy. Although such a ground-state analysis provides merely a necessary condition of the stability for an Ising system and does not fully justify the applicability to a realistic alloy system, a set of effective cluster interaction energies obtained by the present CEM can be regarded as a minimum meaningful set. One way to critically examine the validity of the present set is to carry out the calculation of the phase diagram. Our preliminary study yields 1080 K for the $L1_0$-disorder transition temperature [4] while the experimental value is 1023 K. This is in fairly reasonable agreement and partly resolves the present concern of the convergence of CEM. Yet, it is desirable to investigate the effects of long-range interactions either by employing CPA or by applying the CEM to an extended set of ordered phases. In particular, the former can be combined with Ginzburg–Landau theory to evaluate atomic displacement and ordering energies associated with phase equilibria of two ordered phases with different geometrical lattices [25]. Together with the calculated Fermi surface of a disordered phase, CPA is able to elucidate the electric origin of the phase equilibria.

Within a pair interaction model, the effective pair interaction energy is equivalent to the *interaction parameter* Ω of thermo-chemistry calculations based on the regular solution model [26]. It has been claimed that the sign of Ω uniquely determines the tendency of stability i.e. phase separation for $\Omega < 0$ and ordering for $\Omega > 0$. One can see that this is not the case. Even for positive v_2 over the entire lattice constants covering from Fe to Pd, both phase separation and ordering coexist in the present Fe–Pd system. It should be emphasized that the actual tendency is determined not uniquely by v_2 but by ΔE.

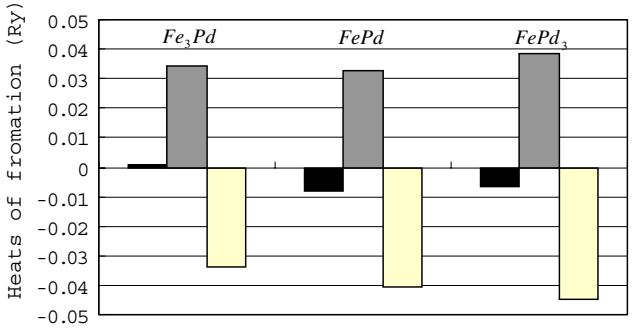

Figure 4. Separation of heats of formation (solid bar) for three ordered phases into elastic (grey bar) and chemical energy (open bar) contributions. The segregation limit is the concentration average of total energies of fcc-Fe (fm) and Pd.

(This figure is in colour only in the electronic version)

It is interesting to separate the heats of formation of an ordered phase n ($= 1$, 2 and 3), $\Delta E_n\,(r_n)$, into the elastic energy contribution, $\Delta E_n^{\rm el}$, and chemical energy contribution, $\Delta E_n^{\rm chem}$, which are defined, respectively, as

$$\Delta E_n^{\rm el} = \Delta E_{\rm Fe}^*(r_n) + \Delta E_{\rm Pd}^*(r_n) \tag{8}$$

and

$$\Delta E_n^{\rm chem} = \Delta E_n^*(r_n) - \Delta E_n^{\rm el}. \tag{9}$$

It is noted that $\Delta E_n^*(r_n)$ are the heats of formation defined with respect to the segregation limit of fcc-Fe (ferro) and Pd, and $\Delta E_n^*(r_n)$ and $\Delta E_n(r_n)$ defined by equation (1) are related through

$$\Delta E_n(r_n) = \Delta E_n^*(r_n) + \frac{4-n}{4}\delta \tag{10}$$

with

$$\delta = E_{\rm Fe_4}(r_0) - E_{\rm Fe_4}^{\rm bcc}(r_{\rm bcc}). \tag{11}$$

Hence, the elastic energy is defined as the energy expended to form a specified ordered compound $\rm Fe_{4-n}Pd_n$ by expanding Fe and contracting Pd to the equilibrium lattice constant r_n, while the chemical energy is the remaining contribution in the heats of formation. The calculated results are shown in figure 4. Note that total, elastic and chemical energies are demonstrated by solid, grey and open bars, respectively, from left to right.

The elastic energy is always positive by definition and this energy causes the phase separation, while the chemical energy is negative for all the phases, which implies that the system has an intrinsically large driving force of ordering. Such a tendency is cancelled by an opposite large contribution of elastic energy for $\rm Fe_3Pd$($n = 1$), resulting in the positive total energy.

The heat of formation for a random solid solution is calculated. At a complete random state, the m-body correlation function $\xi_m^{\rm rand}$ can be given as a simple product (m-tuple) of the point correlation function ξ_1. Hence, equation (3) is transformed for a random solid solution as

$$\Delta E_{\rm rand}(r, x) = \sum_{m=0}^{E_{\rm max}=4} v_m(r)(\xi_1)^m = \sum_{m=0}^{E_{\rm max}=4} v_m(r)(1-2x)^m. \tag{12}$$

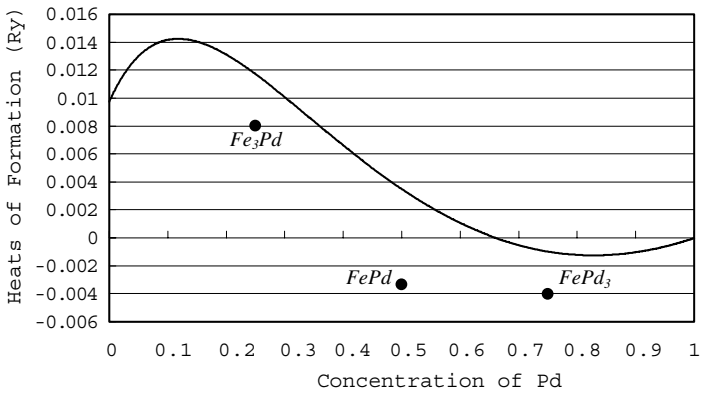

Figure 5. Heats of formation of a complete random solid solution as a function of concentration of Pd. Solid dots indicate the heats of formation of ordered phases (atomic unit).

In the last equality of equation (12), the definition of the point correlation function in terms of concentration of Pd, x, is employed via equation (5). In order to minimize $\Delta E_{\rm rand}(r, x)$ with respect to the lattice constant, we further take a first-order derivative of equation (12) to equate with the external pressure, $p_{\rm ex}$, which is virtually null,

$$\frac{\partial \Delta E_{\rm rand}(r)}{\partial V} = -p = -p_{\rm ex} \cong 0, \tag{13}$$

where the volume, V, is related to the lattice constant through $V = r^3$ for a cubic crystal.

Equations (12) and (13) determine the equilibrium lattice constant $r_{\rm rand}$ and heats of formation $\Delta E_{\rm rand}(r_{\rm rand}, x)$ for a random solid solution as a function of concentration. The concentration dependence of $\Delta E_{\rm rand}(r_{\rm rand}, x)$ is shown in figure 5. Interestingly, the heat of formation is positive in the Fe-rich portion while it is negative in the Pd-rich portion. Together with the positive heats of formation of Fe_3Pd, a strong immiscible tendency is confirmed in the Fe-rich portion. This is believed to lead to the breakdown of the mechanical stability criterion given by $\partial p/\partial V < 0$. The calculation of the pressure–volume curve, however, demands an explicit free energy formula. The details of mechanical stability of the Fe–Pd system are discussed in a future report together with a phase diagram [4].

Finally, densities of states (DOSs) are demonstrated in figures 6(a)–(c) for Fe_3Pd, FePd and $FePd_3$, respectively. A characteristic feature one can observe is that Fermi energy E_F is located near the peak of the DOS for Fe_3Pd, while those of FePd and $FePd_3$ are either in the dip ($FePd_3$) or close to the dip (FePd) of the DOS. The global trend of the phase stability of each ordered phase is, therefore, qualitatively explained by the structure effects of DOS. A quantitative analysis for FePd suggests that the energy difference between E_F and the dip is 0.028 Ryd, which is to be filled by an additional 0.502 electrons (0.112 electrons of up spin and 0.39 electrons of down spin), resulting in the electron per atom ratio of 9.25, which is between 9.0 of FePd and 9.50 of $FePd_3$. If one may take the *rigid-band* view, the analysis above implies that the $L1_0$ ordered phase is more stabilized by increasing the content of Pd. This may provide a clue to understand the shift of congruent composition of the $L1_0$–disorder transition of an experimental phase diagram. We, however, still need more careful analyses including a phase diagram calculation at finite temperatures as well as critical re-assessment of experimental phase diagrams before deriving definite conclusions. These will be undertaken in the subsequent report [4].

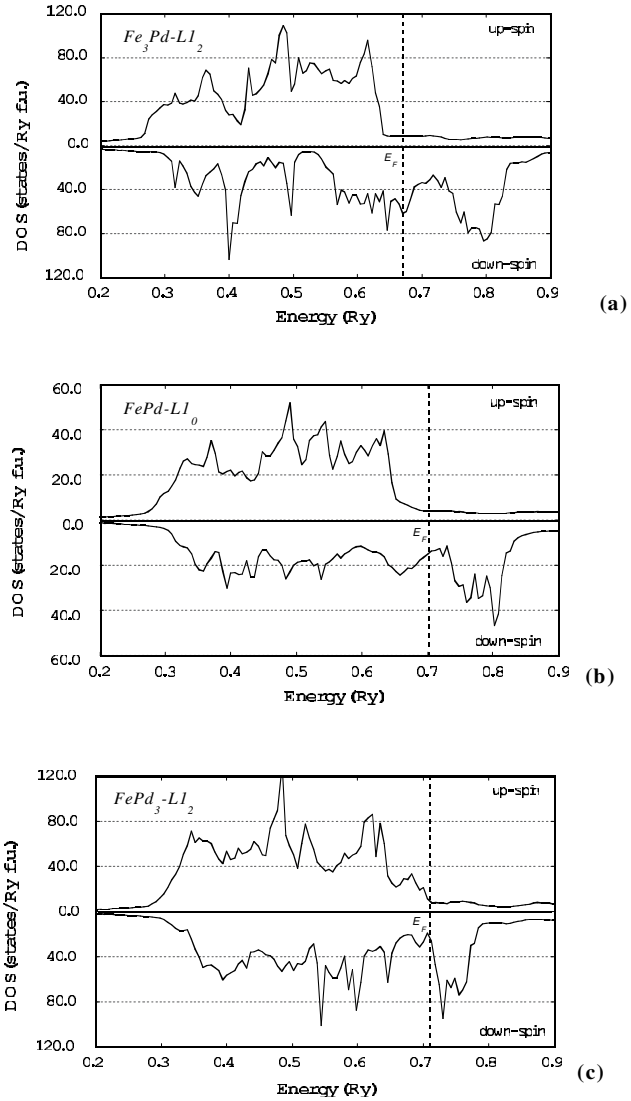

Figure 6. DOS for (*a*) Fe_3Pd, (*b*) FePd and (*c*) $FePd_3$.

Acknowledgment

This work utilized the Database System for Electronic Structures of Japan Science and Technology Corporation (JST).

References

[1] Igarashi S, Muneki S and Abe F 2000 Creep and fracture of engineering materials and structures *Conf. Proc. (Tsukuba)* ed T Sakuma and K Yagi pp 505–12
[2] Mohri T, Horiuchi T, Uzawa H, Ibaragi M, Igarashi M and Abe F 2001 *J. Alloys Compounds* **317/318** 13
[3] Thaddeus B Massalski (ed) 1986 *Binary Alloy Phase Diagrams* (Metals Park, OH: ASM) p 1093
[4] Mohri T, Chen Y and Atago T in preparation

[5] Terakura K, Oguchi T, Mohri T and Watanabe K 1987 *Phys. Rev.* B **35** 2169
[6] Jansen J F and Freeman A J 1984 *Phys. Rev.* B **30** 561
[7] Perdew P, Chevary J A, Vosko S H, Jackson K A, Pederson M R, Singh D J and Fiolhais C 1992 *Phys. Rev.* B **46** 6671
[8] Connolly W and Williams A R 1983 *Phys. Rev.* B **27** 5169
[9] Sanchez J M, Ducastelle F and Gratias D 1984 *Physica* A **128** 334
[10] Sanchez J M and de Fontaine D 1978 *Phys. Rev.* B **17** 2926
[11] Mohri T, Sanchez J M and de Fontaine D 1985 *Acta. Metall.* **33** 1463
[12] Murnaghan F D 1944 *Proc. Natl Acad. Sci. USA* **30** 244
[13] Villars P and Calvert L D 1991 *Pearson's Handbook of Crystallographic Data for Intermetallic Phases* 2nd edn (Metals Park, OH: ASM)
[14] Kittel C 1986 *Introduction To Solid State Physics* 6th edn (New York: Wiley)
[15] Moruzzi V L, Marcus P M and Qiu S L 1995 *Phys. Rev.* B **52** 3448
[16] Correa M H P, Vasquez A and da Silva C E T G 1982 *Solid State Commun.* **42** 251
[17] Hasegawa A 1985 *J. Phys. Soc. Japan* **54** 1477
[18] Galanakis I, Ostanin S, Alouani M and Dreysse H 2000 *Phys. Rev.* B **61** 599
Razee S S, Staunton J B, Johnson D D, Ginatempo B and Bruno E 2001 *J. Phys.: Condens. Matter* **13** 8153
[19] Soven P 1967 *Phys. Rev.* **156** 809
[20] Bieber A, Gautier F, Treglia G and Ducastelle F 1981 *Solid State Commun.* **39** 149
[21] Faulkner J S, Wang Y and Stocks G M 1997 *Phys. Rev.* B **55** 7492
[22] Abrikosov I A, Niklasson A M N, Simak S I, Johansson B, Ruban A V and Skriver H L 1996 *Phys. Rev. Lett.* **76** 4203
[23] Kikuchi R 1951 *Phys. Rev.* **81** 998
[24] Richards M J and Cahn J W 1971 *Acta Metall.* **19** 1263
[25] Bruno E, Ginatempo B and Giuliano S 2001 *Phys. Rev.* B **63** 174107
Gyorffy B L and Stocks G M 1983 *Phys. Rev. Lett.* **50** 374
[26] See, for example, Swalin R A 1972 *Thermodynamics of Solids* (New York: Wiley)